HHS Public Access

Author manuscript

Neurobiol Dis. Author manuscript; available in PMC 2020 December 08.

Published in final edited form as:

Neurobiol Dis. 2020 February ; 134: 104616. doi:10.1016/j.nbd.2019.104616.

Inhibitory designer receptors aggravate memory loss in a mouse model of down syndrome

Eric D. Hamlett[a,*], **Aurélie Ledreux**[b], **Anah Gilmore**[b], **Elena M. Vazey**[c], **Gary Aston-Jones**[d], **Heather A. Boger**[e], **Daniel Paredes**[b,1], **Ann-Charlotte E. Granholm**[b,1]

[a]Department of Pathology and Laboratory Medicine, Medical University of South Carolina, Charleston, SC 29425, USA

[b]Knoebel Institute for Healthy Aging, University of Denver, Denver, CO 80208, USA

[c]Department of Biology, University of Massachusetts Amherst, Amherst, MA 01003, USA

[d]Rutgers Brain Health Institute, Rutgers University, Piscataway, NJ 08854, USA

[e]Department of Neurosciences, Medical University of South Carolina, Charleston, SC 29425, USA

Abstract

The pontine nucleus locus coeruleus (LC) is the primary source of noradrenergic (NE) projections to the brain and is important for working memory, attention, and cognitive flexibility. Individuals with Down syndrome (DS) develop Alzheimer's disease (AD) with high penetrance and often exhibit working memory deficits coupled with degeneration of LC-NE neurons early in the progression of AD pathology. Designer receptors exclusively activated by designer drugs (DREADDs) are chemogenetic tools that allow targeted manipulation of discrete neuronal populations in the brain without the confounds of off-target effects. We utilized male Ts65Dn mice (a mouse model for DS), and male normosomic (NS) controls to examine the effects of inhibitory DREADDs delivered *via* an AAV vector under translational control of the synthetic PRS×8, dopamine β hydroxylase (DβH) promoter. This chemogenetic tool allowed LC inhibition upon administration of the inert DREADD ligand, clozapine-N-oxide (CNO). DREADD-mediated LC inhibition impaired performance in a novel object recognition task and reversal learning in a spatial task. DREADD-mediated LC inhibition gave rise to an elevation of α-adrenoreceptors both in NS and in Ts65Dn mice. Further, microglial markers showed that the inhibitory DREADD stimulation led to increased microglial activation in the hippocampus in Ts65Dn but not in NS mice. These findings strongly suggest that LC signaling is important for intact memory and learning in Ts65Dn mice and disruption of these neurons leads to increased inflammation and dysregulation of adrenergic receptors.

[*]Corresponding author at: Department of Pathology and Laboratory Medicine, Medical University of South Carolina, 173 Ashley Avenue MSC 908, Charleston, SC 29425, USA. hamlette@musc.edu (E.D. Hamlett).

[1]ACG and DP share senior authorship. ACG provided grant funding and senior mentorship for the project, and DP provided mentorship and worked on the manuscript outline and technical aspects.

Declaration of Competing Interest

The authors declare no competing financial interests.

Appendix A. Supplementary data

Supplementary data to this article can be found online at https://doi.org/10.1016/j.nbd.2019.104616.

Keywords

Down syndrome; Locus Coeruleus; Norepinephrine; Designer receptors exclusively activated by designer drugs (DREADD); Alzheimer's disease; Memory; Neuroinflammation

1. Introduction

One of the earliest pathological events in Alzheimer's disease (AD) occurs in the pontine nucleus locus coeruleus noradrenergic (LC-NE) neurons where there is an early accumulation of neurofibrillary tangles (NFTs) (Bondareff et al., 1982; Mann et al., 1984a; Theofilas et al., 2017; Theofilas et al., 2018). A progressive loss of LC neurons ensues, leading to a significant decline in NE levels in LC target regions (Chan-Palay, 1991; Haglund et al., 2006; Kelly et al., 2017) and compensatory changes in adrenoreceptor (AR) levels in terminal fields (Kalaria et al., 1989). Because the LC is prone to early neurodegeneration, it may represent a therapeutic target for AD (Mather and Harley, 2016; Ehrenberg et al., 2017). DS is the most prevalent intellectual disability and affects more than six million people worldwide (Ballard et al., 2016) and 350,000 people in the USA (Zigman,2013). Individuals with DS exhibit a higher prevalence of AD at an earlier age than the general population (Lai and Williams, 1989; Lai, 1992; Menendez, 2005). In addition, neurodegeneration of LC-NE neurons is more severe in people with DS-AD than in the general population (Yates et al., 1981; Mann et al., 1984b, a; Reynolds and Godridge, 1985; Wisniewski et al., 1985a; Godridge et al., 1987; German et al., 1992), and lower levels of NE have been observed in cortical regions by the mid-forties in this population (Yates et al., 1981; Reynolds and Godridge, 1985; Godridge et al., 1987; Risser et al., 1997). Though LC-NE degeneration has significant consequences for AD and DS-AD, little is known about the mechanisms leading to this decline beyond post *mortem* observations.

Several groups have demonstrated that similar LC-NE pathology occurs in mouse models of DS as well as AD. In the DS mouse model, Ts65Dn, LC-NE neuron loss occurs by six months of age (Dierssen et al., 1997; Lockrow et al. 2011; Illouz et al., 2019), along with neurodegeneration of hippocampal, and basal forebrain cholinergic neurons (Reeves et al., 1995; Demas et al., 1996; Escorihuela et al., 1998). Upregulation of β1- and β2-adrenoreceptors (AR) (Salehi et al., 2009; Fortress et al., 2015) along with increased microglial activation (Lockrow et al., 2012) have been observed in Ts65Dn brain and are further exacerbated by neurotoxin-mediated ablation of LC-NE neurons (Lockrow et al. 2011). Importantly, this earlier study by our group demonstrated that the LC-NE plays a significant role in microglial activation and pro-inflammatory cytokine levels in the hippocampus and frontal cortex. The Feinstein group has shown that in addition to an inflammatory surge in the brain, LC-NE lesions also gave rise to increased accumulation of amyloid and exacerbated loss of neurons in Alzheimer's disease (AD) mouse models (Feinstein et al., 2016) thus, ablation of LC-NE represents an important driver in AD pathology. In this study, we were interested in understanding LC function in Ts65Dn mice with a focus on early changes in the LC-NE that may lead to a decline in this system rather than be a consequence of it. Although mouse brain volume is stable at one month of age, maturation remains significant in the first three months, based on recent MRI

characterization (Hammelrath, et at., 2016). After three months, myelination increases slightly in mice, but this change is minor compared to the first three months of maturation. Therefore, to study the adult LC-NE function after maturation and before degeneration, the appropriate age period seems to be 3–6 months in Ts65Dn mice.

It is believed that the tonic NE support to microglial cells and endothelial cells in the brain prevents inflammatory changes. Chronic NE support, such as administration of an agonist to β1-AR (Yi et al., 2017) or the NE precursor L-DOPS (Fortress et al., 2015) in Ts65Dn mice was also sufficient to rescue AR compensatory changes and memory impairments in Ts65Dn mice. In an AD mouse model, treatment with the β1 adrenergic receptor partial agonist Xamoterol prevented memory loss, inflammation and amyloid pathology, strongly suggesting a link between NE signaling and inflammation as well as amyloid production (Ardestani et al., 2017). Microglial cells express both α- and β-adrenergic receptors and are therefore directly affected by the loss of NE tone. Earlier studies by Dierssen et al. demonstrated that downstream adrenergic responses were significantly reduced in cortical regions in Ts65Dn mice already at four months of age (Dierssen et al., 1996). At this age, Dekker et al. recently observed that brain NE levels are normal inTs65Dn mice (Dekker et al., 2017). Collectively, these findings suggest that either adrenoreceptor function, NE synaptic release, or intrinsic LC activity may be dysfunctional. Therefore, an important aim of the current manuscript was to determine whether targeted disruption of the NE activity, rather than the actual loss of neurons and neurites, gave rise to similar changes in inflammatory markers and adrenergic receptors.

Experimentally clarifying LC function *in vivo* presents major challenges. In recent years, the challenges of isolating the effects of intrinsic LC activity in the rodent brain have been overcome by designer receptors exclusively activated by designer drugs (DREADDs), which respond to clozapine N-oxide (CNO) administration *in vivo* (Armbruster et al., 2007; McCall et al., 2015; Roth, 2016; Smith et al., 2016; Mahler and Aston-Jones, 2018). By placing DREADD expression under the control of synthetic PRS×8 dopamine beta-hydroxylase (DβH) promoter, our group and others have successfully used this chemogenetic tool to control LC-NE activity (Vazey and Aston-Jones, 2014; Fortress et al., 2015; Kane et al., 2017). In this study, we utilized PRS×8-hM4Di DREADDs to allow discrete inhibition of the DβH-expressing neurons of the LC without the confounds of neurotoxicity-related neuroinflammation or potential off-target effects from pharmacological approaches. During CNO/hM4Di inhibition of LC-NE activity, we explored several indices of memory, compensatory responses in AR staining density in target regions, and microglial activation associated with LC-NE signaling in mice. We hypothesized that prolonged inhibition of the LC when the animals were young would yield changes in memory performance and aggravate neuroinflammation that occurs with age in this DS mouse model. We also quantified compensatory alterations in adrenergic receptors in response to DREADD inhibition.

2. Materials and methods

2.1. Animal cohorts

Sex differences can significantly affect LC function in regards to stress regulation and vulnerability to elevated corticotropin-releasing factor (Bangasser et al., 2016). To focus on early LC functions while minimizing known gender bias, we conducted this study in male Ts65Dn mice ($n = 15$) and male littermate normosomic (NS) controls ($n = 13$) obtained from Jackson Laboratories (Bar Harbor, ME). Ts65Dn mice are partially trisomic for a segment of murine chromosomes 16 and 17 as described in detail previously (Davisson et al., 1990; Hamlett et al., 2016), have normal visual function (Costa et al., 2010) and have been used by our laboratory routinely (Granholm, 2000; Hunter et al., 2004; Lockrow et al., 2011; Fortress et al., 2015). All mice were single-housed, received food and water *ad libitum* were maintained on a 12-h light/dark cycle and received AAV injections at 12 weeks of age (Fig. 1). All experimental procedures were approved by the Institutional Animal Care and Use Committee (IACUC) of the Medical University of South Carolina in accordance with the guidelines described in the US National Institutes of Health Guide for the Care and Use of Laboratory Animals.

2.2. AAV and construct design

The PRS×8 promoter, a synthetic construct based on the binding motif for the transcription factors Phox2a/2b (Hwang et al., 2001), was used to limit the expression of DREADD hM4Di to cells that actively transcribe the DβH enzyme (Alexander et al., 2009). This hM4Di construct has recently been utilized by others and shown to significantly decrease firing rates in LC neurons during CNO administration (McCall et al., 2015). For LC inhibition studies, eight NS mice and ten Ts65Dn mice received the AAV-hM4Di construct. For sham control studies, the constitutively active cytomegalovirus (CMV)-promoter was used to drive expression of GFP in a separate AAV construct injected into groups of Ts65Dn and NS mice. For proper sham controls, five NS mice and five Ts65Dn mice received the AAV-GFP construct. All vectors were cloned and packaged at the Penn Vector Core (University of Pennsylvania, Philadelphia, PA) specifically with AAV2/9 serotype to promote efficient transduction of neurons (Aschauer et al., 2013). AAV viral particle concentrations were 4.5 × 1012 gc/ml (AAV-PRS×8-hM4Di) and 2×10^{12} gc/ml (AAV-CMV-GFP).

2.3. Experimental design

At three months of age, all mice were anesthetized with ketamine: xylazine (120 mg/kg: 6 mg/kg, i.p.) and given a long-acting local anesthetic in the skin overlying the injection site (bupivacaine, 1 mg/kg, subcutaneous) prior to surgery. Anesthetized mice were placed in a rodent stereotaxic apparatus with a mouse adaptor, and intracranial injections of AAV were delivered bilaterally into the pontine LC by a Hamilton syringe at the following stereotaxic coordinates: −5.34 mm AP, −2.5 mm DV (from the brain surface), ± 1.0 mm from Bregma (Paxinos and Franklin, 2001). Packaged AAV was delivered at a rate of approximately 0.1 μl per minute over ten minutes for a total volume of 1.0 μl per injection site. After microinjection, the syringe was left in place for 10 min to limit backflow diffusion into the injection track. Animals were then sutured, removed from the stereotaxic apparatus, and

monitored for a full recovery before returning to disposable cages housed in a BSL2 room. Intracranial injections occasionally puncture cerebellar arteries in the brain stem resulting in a surgical loss rate of 13% within the procedure. Three weeks of recovery time were allowed for healing and DREADD receptor translation as assessed in DβH-expressing LC neurons that also stain positive for tyrosine hydroxylase (TH) as outlined in Fig. 1 above.

All behavioral testing was conducted over two weeks at 4 months of age, as outlined in Fig. 1A above. Mice received intraperitoneal (i.p.) injections of 0.3 mg CNO (Sigma, St. Louis MO) in saline per kg of total body weight, or injection of saline alone, 10 min before the start of behavioral testing, according to previously published protocols (Alexander et al., 2009; Fortress et al., 2015). Although CNO can be metabolized to clozapine leading to behavioral effects in rodents at higher doses (Manvich et al., 2018), work by our group and our collaborators has shown that doses up to 10 mg/kg of CNO does not exert behavioral effects (Vazey and Aston-Jones, 2014; Kane et al., 2017) and that the dose of CNO utilized herein (0.3 mg/kg) is sufficient to elicited robust effects in AAV-hM4Di-injected but not in AAV-GFP injected mice. Mice from all four experimental groups (NS GFP, NS hM4Di, Ts65Dn GFP and Ts65Dn hM4Di) received either CNO or saline injections in a randomized order. Following dosing, mice were placed in locomotor activity chambers for 1 h (for habituation). The following day, all mice were given respective injections again and evaluated in a 2-day novel object recognition task (NORT). After a two-day period to ensure CNO clearance (Guettier et al., 2009; Fortress et al., 2015), the treatments were switched for each mouse followed by a second measure of locomotor activity, habituation and NORT memory testing. The following three days, all mice received CNO (0.3 mg/kg) daily and were evaluated in a water radial arm maze task (WRAM). After behavioral tasks, all mice received CNO (0.3 mg/kg) daily for three days to ensure that each study cohort underwent CNO-mediated DREADD activation for six consecutive days.

2.4. Spontaneous locomotor activity

Spontaneous activity was measured using the Digiscan Animal Activity Monitor system, and horizontal and vertical activity were collected as described previously (Boger et al., 2006; Fortress et al., 2015). Briefly, mice were placed in a darkened testing chamber and allowed to move freely through photobeam breaks in the X, Y, and Z axes for one hour. Data were analyzed using VersaMAX software version 4.0–137E (Accuscan Instruments, Columbus, OH).

2.5. Novel object recognition task (NORT)

The NORT is a working memory task based on familiar and novel object recognition. We have previously utilized the NORT in Ts65Dn mice, showing a significant deficit in discrimination of novel *vs*. familiar objects, both after a short and long delay interval (Lockrow et al. 2011). On trial day one, mice were placed in the testing arena (40 cm × 40 cm wide × 30 cm high) for a period of ten minutes with no object for habituation purposes. On the next day of testing, mice were placed in the chamber with two identical objects placed in the midline equidistant from each other and the walls (approx. 8 cm radial clearance). Interactions with both objects were recorded for 15 min with a digital video camera mounted overhead. After a 90-min inter-trial delay, mice were placed in the chamber

with two objects: a familiar object from the preceding set and a novel object. The same procedure was repeated after 24 h, with again one familiar and one novel object introduced in the same testing arena. Interactions with both objects were recorded for 15 min. The spatial location for the objects remained the same throughout testing. Videos were scored for the duration of time spent with each object by a blinded observer. For each study, two dependent measures were calculated: the percent time with the novel object and the discrimination index (DI) (Lockrow 2011), which represents the net time spent with the novel object relative to the total time spent with both objects.

2.6. Water radial arm maze (WRAM)

A water radial arm maze (WRAM) is a non-appetitive task that can be used for testing spatial learning and memory even in aged or otherwise compromised mice since water motivates escape with nearly 100% completion of the task (Cravens, 1974; Alamed et al., 2006). The WRAM utilized here was a three-day spatial memory task in which one platform in an eight-arm maze was kept in the same position throughout testing using a win-stay paradigm. The platform was placed approximately 1 cm below the water surface, as previously described (Lockrow et al. 2011). On each day, twelve trials were run as two blocks of six trials, with only six mice per trial block, which permitted a short inter-trial interval rest (five min). On day three, after spatial memory testing and a resting period of 45 min, a cognitive flexibility task was implemented by moving the hidden platform to a new arm location while extra-maze cues remained unchanged. Perseverance to the original platform location and total incorrect arm entries were counted in two blocks with four trials each as described above. After one minute, the mice were gently guided to the new platform location to reinforce the new position. Errors from four trials were summed into one block resulting in comparisons of consecutive blocks for each task (start-mid-end) for spatial memory or (start-end) for cognitive flexibility.

2.7. Tissue preparation and immunostaining

After behavioral testing, all mice were euthanized using an overdose of isoflurane. Brains were rapidly dissected and then placed into 4% paraformaldehyde for 48 h for immersion fixation, then placed into 30% sucrose in PBS for at least 72 h before sectioning at 40 μm on a Microm cryostat (Thermo Fisher Scientific Inc., Waltham, MA). Sections containing hippocampus, parietal cortex, entorhinal cortex, and the pontine region containing the LC were immunostained by DAB as previously described (Fortress et al., 2015).

DREADD/LC colocalization confirmation was performed on 3–4 animals per hM4Di cohort. A series of every sixth section was blocked for one hour in 10% normal goat serum (NGS)/ 0.25% Triton X-100 in TBS Sections were incubated overnight at room temperature with anti-tyrosine hydroxylase (TH) (#P40101–150, dil. 1:1000, Pel-Freeze, Rogers, AR) and anti-hemagglutinin (HA1.1) antibodies (#3724, dil. 1:1000, Cell Signaling Technologies, Danvers, MA). For adrenoreceptor studies, immunostaining was performed on 5–7 animals per cohort with sections representing the hippocampus, parietal (PAR) and entorhinal (ENT) cortical regions. Since some human AR antibodies have demonstrated non-specificity (Hamdani and van der Velden, 2009;Jensen et al., 2009), we utilized antibodies that have been developed for mouse ARs and demonstrated to have reactivity to a

singular band by membrane (Perez et al., 1993; Pullar et al., 2006; Gilbert et al., 2014). A control blocking peptide specific to each AR was also employed to further confirm antibody binding specificity. For ARs, sections were incubated overnight at room temperature with anti-β1 (#AAR-023, dil. 1:400), anti-β2 (#AAR-016, dil. 1:200), anti-β3 (#AAR-017, dil. 1:100), anti-α1a (#AAR-015, dil. 1:100), anti-α2a (#AAR-020, dil. 1:200), anti-α2b (#AAR-021, dil. 1:100), or anti-α2c (#AAR-021, dil. 1:100) AR antibodies with or without blocking peptides at the recommended concentrations (Alomone Labs, Jerusalem, Israel).

For LC morphological characterization, immunostaining was performed on 4–5 animals per cohort with sections representing every sixth section of LC was incubated overnight at room temperature with anti-TH (or #AB113, dil. 1:100, Abcam, Cambridge, MA). Synapse marker immunostaining was performed on 4–5 animals per cohort with matched hippocampal sections. Each section was incubated overnight at room temperature with anti-synapsin (#AB1543, dil. 1:500, Millipore, Burlington, MA). Microglial immunostaining was performed on 5–7 animals per cohort. Matched sections from various regions were incubated overnight at room temperature with anti-CD45 (#MCA1388, dil. 1:200, Bio-Rad, Hercules, CA). After washing, sections were incubated for one hour with secondary antibodies directed against the appropriate species that were conjugated with tetramethylrhodamine (TRITC), with fluorescein isothiocyanate (FITC, 1:200, Jackson Immunoresearch, West Grove, PA) or with biotin. For biotin-conjugated secondary antibodies, sections were then incubated with ABC solution for DAB signal amplification (Vector, Burlingame, CA) followed by development with DAB (Sigma, St. Louis, MO).

The stained tissues were mounted onto slides, dehydrated, and cover-slipped with ProLong Gold Antifade Mountant (Fisher Scientific, Fair Lawn, NJ). All images were captured using a Nikon Eclipse 80i microscope (Nikon Instruments, Melville, NY) equipped with a Qcam digital camera or with an Olympus confocal laser scanning microscope equipped with FlowView FV3000 software (Olympus, Tokyo, Japan) with 16-bit grayscale with 65,000 shades of grey. For confocal images, the immunofluorescence (IF) intensity in each Z-plane stack was summed without further manipulation. Average fluorescence intensity was quantified from each region of interest over 3–4 sections for each animal, with background subtraction performed on unstained areas of each section. Average fluorescence intensity was quantified with freely available FIJI software version 1.52c (Rueden et al., 2017). For normalized data, the control NS GFP group average was set at 1.0 and all other data was adjusted to that normative value.

3. Statistical analysis

To rule out effects of surgery or stereotactic injections on behavior, we first performed a one-way ANOVA to test for significant differences between GFP groups that received either saline or CNO treatment (controls) and the hM4Di group that received saline treatment (inactive). We used Tukey's *post hoc* analysis to examine statistical patterns that were not specified *a priori*. Under these parameters, we observed no significant differences in either NS or Ts65Dn groups for spontaneous activity or NORT (data not shown). Next, we performed two-way ANOVAs to test for differences within AAV groups plus/minus CNO (Karyotype × Treatment). For the 3-day WRAM task, we performed two-way ANOVAs to

test for differences within AAV groups with all receiving CNO (Karyotype × Treatment). Tukey's multiple comparisons tests (with multiplicity-adjusted *p*-values) were used in order to examine statistical patterns that were not specified *a priori* and were reported with an acceptable alpha value of $p < .05$. All correlations were performed using the Pearson correlation matrix. All statistics were performed with GraphPad Prism 7.03 (GraphPad Software, La Jolla, CA) and graphically presented as mean ± SEM.

4. Results

4.1. LC morphology in Ts65Dn mice at 4 months of age

Immunohistochemical quantification of an abundantly expressed LC-NE marker, tyrosine hydroxylase (TH), did not reveal observable alterations in either TH-positive cell bodies or neurites in the LC region in Ts65Dn mice compared to age-matched NS mice ($n = 5$ per cohort) at four months of age (Fig. 1B). Quantification of average TH density within the LC region confirmed that there were no significant differences in terms of TH staining intensity based on a Student's *t*-test between naïve NS and Ts65Dn mice (Fig. 1C, p = .545). This observation suggested that differences in terms of behavior resulting from the CNO-mediated stimulation of DREADDs between NS and Ts65Dn groups would not be due to frank loss of LC-NE neurons in the pontine region.

4.2. AAV transduction of hM4Di DREADDs in LC-NE neurons

AAV was packaged with either a GFP construct, under the control of a CMV promoter, or an HA-tagged DREADD hM4Di construct, under control of the synthetic Dopamine-β-Hydroxylase (DβH) promoter PRS×8 to limit transduction of the AAV to DβH expressing cells (Fig. 2A). We employed bilateral stereotaxic AAV delivery of AAV directly into the LC-NE (Fig. 2B). To confirm AAV transduction success in LC-NE neurons, double labeling of the HA1.1-tagged hM4Di receptor and TH was performed (Fig. 2C). Immunofluorescence revealed that expression of the HA1.1 tag was observed in the LC region in both NS and Ts65Dn mice five weeks post-injection. Co-labeling of HA1.1 and TH and cell counting was undertaken to explore target success and revealed that an average of 98% of TH-positive cells in the LC also co-stained with the HA1.1 tagged DREADD receptor. Sampling was performed in 24 sections both for NS and Ts65Dn groups ($n = 3$ per cohort, the range of co-labeling was 95–100%). The HA-TH double labeling demonstrated that AAV transduction of the DREADD receptors in LC-NE neurons was specific to LC-NE neurons in both NS and Ts65Dn mice. Thus, no mice had to be excluded due to faulty targeting of the AAV vector.

4.3. Spontaneous locomotion

Because hyperactivity has previously been observed in Ts65Dn mice, we examined whether hM4Di-mediated LC inhibition had any effects on spontaneous locomotion in an open field chamber (Fig. 3A). All groups of Ts65Dn mice exhibited significant hyperactivity, regardless of receiving the GFP or DREADD hM4Di constructs and CNO administration had no apparent effects on spontaneous locomotion in any group. To confirm these findings, we performed a two-way ANOVA with Tukey's *post hoc* analyses to test for differences within AAV groups (Karyotype × Treatment). The main effect was attributable to karyotype

alone in both GFP and hM4Di groups. Tukey's post hoc analyses confirmed that CNO administration had no significant effect on hyperactivity in either GFP or hM4Di groups, indicating that inhibition of the LC has no effect on spontaneous locomotion in young mice under our experimental conditions. Since changes in stress or anxiety can affect LC-NE modulation of arousal required to sustain attention for behavioral tasks, we also measured mean velocity and center time in the open field between NS and Ts65Dn mice, and did not observe significant effects from CNO administration or from hM4Di-mediated LC inhibition (data not shown), indicating that our LC manipulations do not affect motor ability or percent center time at four months of age.

4.4. Novel object recognition task

Using the NORT, we first evaluated if LC inhibition at four months of age could affect working memory in NS or Ts65Dn mice when novel objects were introduced at two different intervals: 90 min and 24 h. Under saline treatment, NORT performance was equivalent regardless of whether the mice received AAV-GFP or AAV-hM4Di injections, suggesting that there is no vector delivery impact on mouse behavior (data not shown). We observed that Ts65Dn mice already displayed significant object memory deficits in this task at this age compared to age-matched NS mice and that CNO administration only affected performance in the mice that received the AAV-hM4Di vector. To confirm these findings, we performed a two-way ANOVA with Tukey's multiplicity-adjusted *post hoc* analyses to test for differences within AAV groups (Karyotype × Treatment). At both testing intervals (Fig. 3B–C above), the main effect was attributable to karyotype in all groups and additionally to treatment in the hM4Di groups.

At 90 min, Ts65Dn GFP mice had significant object memory deficits compared to NS mice (Fig. 3B, left), which occurred after administered of saline ($p = .010$) or CNO ($p = .008$). In the hM4Di groups (Fig. 3B, right), Ts65Dn mice already had deficits compared to saline-treated NS mice ($p = .003$). Compared to saline-treatment, CNO-treatment significantly reduced NORT performance in NS mice ($p = .005$). CNO-treated NS mice were not significantly different than saline-treated Ts65Dn mice and CNO-treatment had a marginal effect in Ts65Dn mice since NORT performance was already minimal.

At the 24-h interval in the GFP group (Fig. 3C, left), Ts65Dn mice continued to have significant object memory deficits compared to the NS mice, regardless of treatment (saline, $p = .02$; CNO, $p = .03$). hM4Di-mediated LC inhibition (Fig. 3C, right) significantly decreased NORT performance for NS mice (p = .003). Though the hM4Di Ts65Dn mice already performed significantly worse than NS mice ($p = .04$), they exhibited reduced performance after CNO injections, with a significant reduction in discrimination between the two objects ($p = .017$). Collectively, these findings demonstrated that hM4Di inhibition of LC-NE neurons significantly reduced NORT performance, at both short and long-term intervals, and that NS mice performed no better than Ts65Dn mice when we inhibited LC activity at either 90-min (Fig. 3B, p = .477) or at 24-h (Fig. 3C, p = .239).

4.5. WRAM cognitive flexibility

The WRAM task has longitudinal training effects, so we tested each control group (GFP NS, GFP Ts65Dn) and each experimental group (hM4Di NS, hM4Di Ts65Dn) once with all mice receiving CNO dosing daily. All mice, regardless of experimental condition completed 95% of all swim transits (arm-to-arm) in under 8 s, with no effects of either karyotype or treatment on swimming capability (data not shown), though all Ts65Dn mice demonstrated increased levels of random stalling (inactivity) in the task. As seen in Fig. 4A, both Ts65Dn groups exhibited more errors than both NS groups on all three testing days. Following the last trial of the WRAM task, we examined cognitive flexibility in all groups by switching the platform to a new location and conducting 8 additional trials. When errors were summed over the entire WRAM task (Fig. 4B), Ts65Dn mice made nearly 3-fold more errors than NS mice, regardless of AAV vector received (treatment). To confirm these findings, we performed a two-way ANOVA with Tukey's multiplicity-adjusted *post hoc* analyses to test for differences within AAV groups (Karyotype × Treatment). The main effect was attributable to karyotype, and Ts65Dn performed significantly worse than their NS counterparts (GFP, $p = .006$; hM4Di, $p = .002$). All mice demonstrated high error rates in finding the new hidden platform in the first trial block with variable levels of improvement in the second trial block (Fig. 4C). To confirm these findings, we performed a two-way ANOVA with Tukey's multiplicity-adjusted *post hoc* analyses to test for differences ences within AAV groups (Karyotype × Treatment) on the final trial block. The main effect was attributable to both karyotype and treatment. NS GFP made significantly fewer errors than Ts65Dn GFP (p = .002) and hM4Di inhibition of the LC led to a significant increase in errors for both NS ($p = .042$) and Ts65Dn mice ($p = .004$) when compared to their GFP counterparts. Overall, hM4Di inhibition of the LC did not affect spatial memory performance but interfered with the ability to rapidly learn and target the new platform location after it was moved, demonstrating specific defects of cognitive flexibility caused by CNO-mediated LC inhibition.

4.6. TH staining in the LC

To determine whether chronic DREADD stimulation gave rise to alterations in tyrosine hydroxylase (TH) expression in the LC nucleus or its proximal neurites, we performed immunofluorescence evaluations of TH density in the LC cell body region as well as the neurites surrounding the cell body region (Fig. 5). Although there were no observable differences between any of the groups in terms of cell body staining (Fig. 5 A and C), the fiber density of neurites surrounding the LC was reduced, both as a result of karyotype (NS *vs.* TS) and in terms of treatment (GFP *vs.* hM4DI). (See Fig. 1.)

In the rostral portions of the LC, statistical evaluation of TH fluorescence intensity revealed significant effects of genotype ($F (1, 16) = 7.610$, $p = .0140$) and an interaction between genotype and treatment ($F (1, 16) = 6.935$, $p = .0181$), suggesting that the effects of the inhibitory DREADDs exhibited differential effects in NS *vs.* TS mice (Fig. 5B). In caudal portions of LC, TH fiber density appeared to be less affected in TS mice, since only a significant effect was observed for treatment ($F (1, 16) = 5.038$, $p = .0393$), with no significant interaction between genotype and treatment. These data suggest that TH density in fibers originating in the LC is affected by DREADD inhibition and may, therefore,

influence the expression of, for example, the beta-adrenergic receptors described above. Since LC inhibition could also affect synaptic protein expression and alter the regulation of neurotransmitter release at the synapse, we examined the density of the synaptic protein synapsin in the hippocampal formation. As can be seen in Supplemental Fig. 1, there were no observable or statistical differences between the density of synapsin in any of the groups or hippocampal regions, suggesting that synapse architecture remained intact following the complete twelve day LC inhibition paradigm.

4.7. Adrenoreceptor immunostaining

We hypothesized that hM4Di-mediated LC inhibition in 4-month old mice might lead to AR compensatory responses in LC target regions due to decreased NE activity. We quantified immuno-fluorescence of parietal, entorhinal and hippocampal regions (Fig. 6A) using publicly available annotation (Lein et al., 2007). Overall, α1-AR and α2-AR exhibited increased fluorescence intensity in response to hM4Di-mediated LC inhibition. In addition, α2c-AR staining density was increased in Ts65Dn mice compared to age-matched NS mice, suggesting deficient NE signaling in the DS model at this age. Two-way ANOVAs followed by Tukey's *post hoc* analyses confirmed that hM4Di LC activation resulted in a subtle increase of overall α1a-AR staining in NS mice and significant increases in Ts65Dn mice ($p = .03$, Fig. 6B–C). For α2a-AR immunostaining (Fig. 6D), we observed significant increases in immunostaining for both NS hM4Di and TS hM4Di mice compared to their GFP counterparts ($p = .048$ and $p = .009$, respectively). For α2b-AR immunostaining (Fig. 6E), we observed significant increases in fluorescence intensity for both NS hM4Di and Ts65Dn hM4Di mice ($p = .0004$ and $p < .0001$ respectively). For α2c-AR fluorescence intensity (Fig. 6F), we observed that the Ts65Dn GFP group had significant elevations in fluorescence intensity compared to NS GFP ($p = .003$) and hM4Di-mediated LC inhibition resulted in significant increases in immunostaining for both NS and Ts65Dn mice ($p = .0004$ and $p = .03$, respectively). The greatest changes in immunostaining for all α-ARs were observed in the cortical regions. Cortical regions displayed higher fluorescence intensity while the ENT region displayed the most robust changes in immunostaining in cell bodies and surrounding cellular dendrites in both Ts65Dn and NS hM4Di groups, as shown in (Supplemental Fig. 2). For all α—ARs, only marginal effects were observed in the hippocampus for both NS and Ts65Dn mice (data not shown). The upregulation in α-ARs strongly suggests that the CNO-mediated activation of inhibitory DREADDs gave rise to strongly reduced NE signaling in the target regions, leading to an increased compensatory expression of these NE receptors.

For β-ARs (Fig. 7), Immunostaining revealed that β1-AR and β2-AR fluorescence intensities were increased in the Ts65Dn GFP group, compared to all NS groups and that hM4Di LC inhibition significantly decreased staining in only the Ts65Dn group. β3-AR staining intensity was equivalent in the GFP groups and significantly increased in response to hM4Di inhibition of the LC. To confirm these findings, we performed a two-way ANOVA with Tukey's multiplicity-adjusted post hoc analyses to test for differences within AAV groups (Karyotype × Treatment). For β1- and β2-AR immunofluorescence (Fig. 7B–D), the main effects were attributable to karyotype and treatment with significant interaction since the treatment effect was only observed in Ts65Dn. hM4Di inhibition resulted in a significant

decrease in β1-AR and β2-AR immunostaining only in Ts65Dn mice (p = .0001 and p < .0001, respectively) which was not significantly different than that observed in NS mice. However, for β3-AR immunostaining (Fig. 7E) responded to the hM4Di-mediated LC inhibition with elevated staining, and the main effects were attributable to treatment alone. There was no difference between NS GFP and Ts65Dn GFP groups in β3-AR staining, but hM4Di LC inhibition resulted in significant increases in staining in both NS hM4Di and Ts65Dn hM4Di groups ($p = .006$ and $p = .02$, respectively). We observed changes in fluorescence intensity for all β-ARs in the cortical regions, with the greatest effects seen in the ENT cortical region (Supplemental Fig. 2).

4.8. CD45 immunostaining

CD45 expression is nearly 2-fold higher in disease-associated microglia in the familial onset AD mouse model (Rangaraju et al., 2018) and we have seen similar expression levels in Ts65Dn mice previously (Lockrow et al., 2011a, 2011b). Microscopic evaluation of CD45 immunostaining revealed increased DAB density in activated microglia in the Ts65Dn relative to NS mice, and hM4Di LC inhibition further increased staining levels in both NS and Ts65Dn mice in the hippocampus (Fig. 8A), parietal (Fig. 8B–C) and frontal (Fig. 7D) cortical regions. To confirm these findings, we performed a two-way ANOVA with Tukey's *post hoc* analyses to test for differences within AAV groups (Karyotype × Treatment). The main effects were attributable to karyotype and treatment for both frontal and parietal cortical regions. In the parietal cortex (Fig. 8D). Tukey's *post hoc* analyses revealed that Ts65Dn GFP mice had significantly greater CD45 density that NS GFP mice ($p = .007$). hM4Di LC inhibition significantly elevated CD45 density. in the Ts65Dn.hM4Di group relative to the Ts65Dn GFP group ($p = .027$). In the frontal cortex, Tukey's *post hoc* multiple comparison tests confirmed that Ts65Dn mice had significantly greater CD45 DAB density than NS GFP mice ($p = .014$, Fig. 8D). The hM4Di cohorts resulted in increased levels of CD45 density for both NS ($p = .003$) and Ts65Dn mice ($p = .04$), with almost three-fold higher density than that observed in the NS GFP mice.

To investigate whether activation of microglia was related to performance in the behavioral tasks, we performed Pearson's correlations and determined that CD45 DAB density in the frontal cortex region was significantly correlated with the NORT discrimination index (*negative correlation*) at the 24-h interval ($r = −0.459$, $p = .021$ and $r = −0.548$, $p = .005$, respectively, see Fig. 8F). This indicates that the hM4Di Ts65Dn mice which exhibited the most elevated CD45 staining performed worse on this working memory task. Moreover, CD45 staining in the frontal cortex also positively correlated with overall α1a-($r = 0.743$, $p = .0002$), α2a- (r = 0.743, p = .0002), α2b- ($r = 0.494$, p = .027) and α2c-AR ($r = 0.685$, $p = .0009$) staining intensities, suggesting a potential role of α-AR expression on activation of microglial cells. Altogether, these findings suggest that DREADD inhibition of LC-NE exacerbates neuroinflammation as observed by CD45 expression with observations of a higher frequency of activated microglia phenotypes in both NS and, to a greater extent, in Ts65Dn mice.

5. Discussion

The findings presented here demonstrate the role of the LC in specific memory domains and in resident microglial status in Ts65Dn mice. Correlation studies strongly indicate that microglial activation is related to memory loss and to elevations in a-ARs occurring following the CNO-mediated DREADD stimulation. In this study, we confirmed that LC morphology was equivalent between NS and Ts65Dn mice as evidenced by TH immunostaining at 4 months of age (Fig. 1B & Fig. 5), as previously reported by our group (Lockrow et al. 2011). NS mice that received AAV-delivery of hM4Di DREADD exhibited reduced discrimination in the NORT upon administration of CNO, both at 90-min and 24-h inter-trial intervals. Similar observations were made in Ts65Dn mice though less pronounced, due to a ceiling effect. Although we did not perform electrophysiological recordings of LC-NE firing rates in the current study, the same hM4Di DREADD construct has been shown to facilitate tonic neuronal inhibition with 60–85% reduction of spontaneous action potentials, using electrophysiological recordings, in neurons found in the ventral pallidum (Mahler et al., 2014), in parvalbumin-expressing (Nguyen et al., 2014) or glutamatergic neurons (Lopez et al., 2016) found in the hippocampus, and in the principal neurons of the basolateral amygdala (Lopez et al., 2016). Further, the strong compensatory increase in alpha-adrenoreceptor immunostaining (Fig. 6) observed in both genotypes following CNO-hM4Di stimulation provides indirect proof for reduced NE signaling. Behavioral deficits from LC inhibition were correlated with alterations in immunostaining of ARs and to CD45 expression in microglia but are not attributable to changes in synapse architecture given that we observed no changes in synapsin in any cohort examined (Suppl. Fig. 1).

It has been unclear from the literature whether direct signaling of LC-NE neurons is involved in spatial reference memory in rodents. Collier and collaborators showed that aged rats with reduced cortical NE activity exhibited reduced spatial reference learning and memory (Collier et al., 2004). This corroborates a previous study from our group, where we found that the selective NE neurotoxin, DSP4, significantly aggravated both spatial and working memory in Ts65Dn mice, but not in age-matched NS mice. However, it is not clear from previous studies whether Ts65Dn mice have early deficits in NE signaling that might lead to LC-NE neurodegeneration with age. The reaction to CNO-mediated hM4Di activation reported herein demonstrated altered response as well as aggravation of microglial activation following hM4Di-mediated LC inhibition. Bilateral lesions of the LC in rats has been shown to severely impair spatial memory acquisition in a water maze task (Khakpour-Taleghani et al., 2009). But, some reports have shown that chemical lesions of the NE system do not impair spatial memory in young and unimpaired rodents, suggesting that an already sensitized brain may be more susceptible to damage (Langlais et al., 1993; Benloucif et al., 1995). In this study, neither spatial reference memory nor spontaneous locomotion were affected by hM4Di-mediated inhibition of LC-NE signaling, possibly due to the fact that the study was performed in young mice, who did not exhibit LC-NE degeneration and do not have chronic LC dysfunction. However, hM4Di LC inhibition reduced cognitive flexibility in both NS and Ts65Dn mice in the WRAM during the reversal task suggesting that this more specific cognitive task was vulnerable to the reduced LC-NE signaling.

NORT performance was significantly affected by hM4 LC-inhibition, particularly in NS mice. Entorhinal cortical areas provide object-based information and novelty/familiarity information for the hippocampus, which is demonstrated clearly upon entorhinal lesion (Kinnavane et al., 2016). Here we have demonstrated that, upon LC inhibition, the most robust AR responses were quantified in the ENT region (Suppl. Fig. 2) Collectively, this result adds to the converging evidence that ENT—hippocampal circuits are critical for episodic memory and temporal associative learning that is necessary for the NORT task. The significant correlation between α2-AR immunostaining and NORT performance suggested that expression levels of adrenoreceptor subtypes may play a role for object memory recognition in all mice. All three of the known subtypes of the α2-adrenergic receptor are linked to inhibition of adenylyl cyclase activity, which is required for novelty recognition (Wang et al., 2011). In radioisotope studies, Dierssen et al. discovered that cyclic adenosine monophosphate (cAMP) accumulation upon administration of isoprenaline or forskolin (both 10 μM) was significantly reduced in the hippocampus and cerebellar cortex in 5–7 months of age Ts65Dn mice (Dierssen et al., 1996; Baamonde et al., 2011), providing a potential mechanism for the observed alterations reported herein. Here we demonstrate that α2c-AR showed increased immunostaining in many cortical regions in Ts65Dn mice even without CNO stimulation. Given the profound NORT dysfunction seen in Ts65Dn mice, we speculate that overactive synaptic auto-regulatory functions could be playing a role in the Ts65Dn behavioral phenotype. Recently, several highly selective α2c-AR antagonists have been identified that have been shown to have pro-cognitive actions in animals (Uys et al., 2017). One α2c-AR antagonist, ORM-12741, is already in clinical development for the treatment of cognitive dysfunction and neuropsychiatric symptoms in AD, suggesting a potential target for intervention also in people with Down syndrome.

We have previously shown that Ts65Dn mice have increased immunostaining of β1-AR at 11–13 months compared to age-matched NS mice (Fortress et al., 2015) and that treatment with the NE precursor L-DOPS normalized β1-AR expression. At a similar age, Salehi et al. also observed significant elevations in β2-AR expression in Ts65Dn mice (Salehi et al., 2009). Since LC morphology is intact in Ts65Dn mice at 4 months of age, we presumed that all AR immunostaining would be similar between NS-GFP and Ts65Dn-GFP mice in terminal fields including the hippocampus, parietal and/or entorhinal cortex. Confirming this hypothesis, previous radioisotope-enabled studies suggested thatβ-AR levels in the cortex of Ts65Dn mice (Dierssen et al., 1997) are not significantly different than levels seen in NS mice. Contrary to this hypothesis, we here observed significant elevations in β1-andβ2-AR fluorescent immunostaining in LC target regions between Ts65Dn and NS mice at 4 months of age. These results may suggest that Ts65Dn mice have an undefined deficit in NE function much earlier than previously known and preceding frank degeneration of LC-NE neurons. We originally hypothesized that hM4Di inhibition of LC-NE activity would give rise to increased AR staining in LC-NE target regions due to depletion of NE, similar to the effects seen from the administration of reserpine (Bylund et al., 1981). As expected, staining intensity of most adrenoreceptors was increased by hM4Di LC inhibition in cortical regions for both NS and Ts65Dn mice as seen from fluorescence intensity quantification in (Fig. 5).

However, unlike β3- and α-ARs, the β1- and β2-ARs were unresponsive in NS mice and responded to the hM4Di-mediated LC inhibition with reduced immunostaining in Ts65Dn

mice, rather than an increase in staining, as was seen with the other receptor subtypes. Interestingly, microglial cells express both β1- and β2-ARs and activation of these receptors protects microglia against oligomeric amyloid-beta in tissue culture (Xu et al., 2018). Although Ts65Dn mice do not accumulate amyloid pathology (Holtzman et al., 1996), they do display age-related elevation of APP and oligomeric amyloid-beta in the hippocampus (Hunter et al., 2003; Sansevero et al., 2016). This increased oligomeric amyloid-beta could, therefore, be the primary reason why β-AR receptor levels are upregulated in the Ts65Dn mouse during normal conditions. However, if these receptors are dysfunctional, as occurs in the cessation of NE signaling, a downregulation would instead aggravate amyloid toxicity. Analysis of adrenergic receptor expression with quantitative PCR has shown that resting microglia primarily express β2 receptors but switch expression to β2A receptors under pro-inflammatory conditions modeled by LPS treatment (Gyoneva and Traynelis, 2013). This switch from beta- to alpha-adrenergic response could explain our findings resulting from the CNO-DREADD activation and would support the notion that upregulation of expression of alpha-ARs could play a role for the elevated microglial activation which was observed in the current study.

We have previously shown that Ts65Dn mice exhibit an age-related progressive increase in microglial activation relative to NS mice (Lockrow et al., 2012) coupled with increased levels of pro-inflammatory cytokines (IL-1β) — changes which are further exacerbated with neurotoxin-mediated lesions of the LC (Lockrow 2011). hM4Di-mediated LC inhibition significantly increased CD45 immunostaining in both NS and Ts65Dn groups, thus aggravating existing neuroinflammation in the Ts65Dn mice, and concurrent data showing elevated alpha receptors suggest an interaction between increased microglial activation and adrenergic receptor expression. This finding fits well with clinical studies, showing elevated pro-inflammatory cytokines in blood samples from both children and adults with DS (Trotta et al., 2011; Cavalcante et al., 2012), as well as in the Ts65Dn mouse model (Fructuoso et al., 2018). In this study, all animals received daily injections (for up to 12 days) of CNO which was sufficient to accelerate an inflammatory phenotype. Since the LC-NE neurons innervate both microglial cells and astrocytes (Kong et al., 2010), depletion of NE signaling in target regions leads to an alteration of the inflammatory homeostasis. This has also been observed in mouse models of AD (Feinstein et al., 2002; Kalinin et al., 2007; Feinstein et al., 2016). It is well known that microglial activation in the brain occurs years before the appearance of Aβ plaques in humans with DS (Wisniewski et al., 1985b). The fact that CD45 immunostaining correlated with behavioral measures provides further evidence for the important role of inflammatory homeostasis in DS.

The findings in the current work add to the understanding of the LC-NE role for maintenance of working memory function, neuroin-flammation, and homeostasis in the DS brain. Additionally, AAV-delivered DREADDs provide an elegant tool for assessing discrete functions of individual neuronal signaling for pathology without the confounds of neurotoxicity-related neuroinflammation or potential off-target effects from pharmacological approaches. We would like to emphasize that future studies utilizing both male and female mice might reveal sex differences not only in general baseline memory impairments for Ts65Dn at 4 months of age, but also in gender response to this unique method of LC inhibition. This is an important matter as many rodent studies have shown sex differences

can affect LC functions in regards to stress regulation and vulnerability to elevated corticotrophin-releasing factor (Bangasser et al., 2016). There is an urgency for the development of novel therapeutic targets for the increasing number of aging adults with DS that have a high prevalence for AD. The current findings provide a more in depth understanding of how Trisomy 21 affects the NE transmitter system and future studies will be focused on developing novel therapeutic interventions targeting this important transmitter system.

Supplementary Material

Refer to Web version on PubMed Central for supplementary material.

Acknowledgments

The authors would like to thank Ms. Laura Columbo for excellent technical assistance with the project. The authors would like to thank Dr. Bryan Roth from the University of North Carolina at Chapel Hill, NC for providing the DREADD-hM4Di construct, and Hammam Belgasem for technical assistance.

This work was supported by the Alzheimer's Association [DSADIIP-13-284845] and a grant from the Foundation LeJeune USA to ACG.

Abbreviations:

MHPG	3-methoxy-4-hydroxyphenylglycol
AAV	Adeno-associated virus
AR	Adrenoreceptor
ANOVA	Analysis of variance
AD	Alzheimer's disease
CNO	Clozapine-N-oxide
cAMP	Cyclic adenosine monophosphate
CMV	Cytomegalovirus
DREADDs	Designer receptors exclusively activated by designer drugs
DAB	Diaminobenzidine tetrahydrochloride
DβH	Dopamine β hydroxylase
DS	Down syndrome
ENT	Entorhinal
GFP	Green fluorescent protein
HA	Hemagglutinin
hM4Di	Human muscarinic receptor 4 DREADD

L-DOPS	L-Dihydroxyphenylserine
LC-NE	Locus coeruleus noradrenergic
NFTs	Neurofibrillary tangles
NE	Norepinephrine
NS	Normosomic
NORT	Novel object recognition task
PAR	Parietal
SEM	Standard error of the mean
TH	Tyrosine hydroxylase
WRA	Water radial arm maze

References

Alamed J, Wilcock DM, Diamond DM, Gordon MN, Morgan D, 2006 Two-day radial-arm water maze learning and memory task; robust resolution of amyloid-related memory deficits in transgenic mice. Nat. Protoc 1, 1671–1679. [PubMed: 17487150]

Alexander G, Rogan C. Sarah, Abbas I. Atheir, Armbruster N. Blaine, Ying Pei, Allen A. John, Nonneman J. Randal, Hartmann John, Moy S. Sheryl, Nicolelis MA, 2009 Remote control of neuronal activity in transgenic mice expressing evolved G protein-coupled receptors. Neuron 63, 27–39. [PubMed: 19607790]

Ardestani PM, Evans AK, Yi B, Nguyen T, Coutellier L, Shamloo M, 2017 Modulation of neuroinflammation and pathology in the 5XFAD mouse model of Alzheimer's disease using a biased and selective beta-1 adrenergic receptor partial agonist. Neuropharmacology 116, 371–386. [PubMed: 28089846]

Armbruster BN, Li X, Pausch MH, Herlitze S, Roth BL, 2007 Evolving the lock to fit the key to create a family of G protein-coupled receptors potently activated by an inert ligand. Proc. Natl. Acad. Sci. U. S. A. 104, 5163–5168. [PubMed: 17360345]

Aschauer DF, Kreuz S, Rumpel S, 2013 Analysis of transduction efficiency, tropism and axonal transport of AAV serotypes 1, 2, 5, 6, 8 and 9 in the mouse brain. PLoS One 8, e76310. [PubMed: 24086725]

Baamonde C, Martinez-Cue C, Florez J, Dierssen M, 2011 G-protein-associated signal transduction processes are restored after postweaning environmental enrichment in Ts65Dn, a down syndrome mouse model. Dev. Neurosci. 33, 442–450. [PubMed: 21865666]

Ballard C, Mobley W, Hardy J, Williams G, Corbett A, 2016 Dementia in Down's syndrome. Lancet Neurol. 15, 622–636. [PubMed: 27302127]

Bangasser DA, Wiersielis KR, Khantsis S, 2016 Sex differences in the locus coeruleus-norepinephrine system and its regulation by stress. Brain Res. 1641 (Pt B), 177–188 615. [PubMed: 26607253]

Benloucif S, Bennett EL, Rosenzweig MR, 1995 Norepinephrine and neural plasticity: the effects of xylamine on experience-induced changes in brain weight, memory, and behavior. Neurobiol. Learn. Mem 63, 33–42. [PubMed: 7663878]

Boger HA, Middaugh LD, Huang P, Zaman V, Smith AC, Hoffer BJ, Tomac AC, Granholm AC, 2006 A partial GDNF depletion leads to earlier age-related deterioration of motor function and tyrosine hydroxylase expression in the substantia nigra. Exp. Neurol. 202, 336–347. [PubMed: 16889771]

Bondareff W, Mountjoy CQ, Roth M, 1982 Loss of neurons of origin of the adrenergic projection to cerebral cortex (nucleus locus ceruleus) in senile dementia. Neurology 32, 164–168. [PubMed: 7198741]

Bylund DB, Forte LR, Morgan DW, Martinez JR, 1981 Effects of chronic reserpine administration on beta adrenergic receptors, adenylate cyclase and phosphodiesterase of the rat submandibular gland. J. Pharmacol. Exp. Ther. 218, 134–141. [PubMed: 6113277]

Cavalcante LB, Tanaka MH, Pires JR, Apponi LH, Aparecida Giro EM, Valentini SR, Palomari Spolidorio DM, Capela MV, Rossa C Jr., Scarel-Caminaga RM, 2012 Expression of the interleukin-10 signaling pathway genes in individuals with down syndrome and periodontitis. J. Periodontol. 83, 926–935. [PubMed: 22050548]

Chan-Palay V, 1991 Alterations in the locus coeruleus in dementias of Alzheimer's and Parkinson's disease. Prog. Brain Res. 88, 625–630. [PubMed: 1726030]

Collier TJ, Greene JG, Felten DL, Stevens SY, Collier KS, 2004 Reduced cortical noradrenergic neurotransmission is associated with increased neophobia and impaired spatial memory in aged rats. Neurobiol. Aging 25, 209–221. [PubMed: 14749139]

Costa AC, Stasko MR, Schmidt C, Davisson MT, 2010 Behavioral validation of the Ts65Dn mouse model for down syndrome of a genetic background free of the retinal degeneration mutation Pde6b(rd1). Behav. Brain Res. 206, 52–62. [PubMed: 19720087]

Cravens RW, 1974 Effects of maternal undernutrition on offspring behavior: incentive value of a food reward and ability to escape from water. Dev. Psychobiol. 7, 61–69. [PubMed: 4812271]

Davisson MT, Schmidt C, Akeson EC, 1990 Segmental trisomy of murine chromosome 16: a new model system for studying down syndrome. Prog. Clin. Biol. Res. 360, 263–280. [PubMed: 2147289]

Dekker AD, Vermeiren Y, Albac C, Lana-Elola E, Watson-Scales S, Gibbins D, Aerts T, Van Dam D, Fisher EMC, Tybulewicz VLJ, Potier MC, De Deyn PP, 2017 Aging rather than aneuploidy affects monoamine neurotransmitters in brain regions of down syndrome mouse models. Neurobiol. Dis. 105, 235–244. [PubMed: 28624415]

Demas GE, Nelson RJ, Krueger BK, Yarowsky PJ, 1996 Spatial memory deficits in segmental trisomic Ts65Dn mice. Behav. Brain Res. 82, 85–92. [PubMed: 9021073]

Dierssen M, Vallina IF, Baamonde C, Lumbreras MA, Martinez-Cue C, Calatayud SG, Florez J, 1996 Impaired cyclic AMP production in the hippocampus of a down syndrome murine model. Brain Res. Dev. Brain Res. 95, 122–124. [PubMed: 8873983]

Dierssen M, Vallina IF, Baamonde C, Garcia-Calatayud S, Lumbreras MA, Florez J, 1997 Alterations of central noradrenergic transmission in Ts65Dn mouse, a model for down syndrome. Brain Res. 749, 238–244. [PubMed: 9138724]

Ehrenberg AJ, Nguy AK, Theofilas P, Dunlop S, Suemoto CK, Di Lorenzo Alho AT, Leite RP, Diehl Rodriguez R, Mejia MB, Rub U, Farfel JM, de Lucena Ferretti-Rebustini RE, Nascimento CF, Nitrini R, Pasquallucci CA, Jacob-Filho W, Miller B, Seeley WW, Heinsen H, Grinberg LT, 2017 Quantifying the accretion of hyperphosphorylated tau in the locus coeruleus and dorsal raphe nucleus: the pathological building blocks of early Alzheimer's disease. Neuropathol. Appl. Neurobiol. 43, 393–408. [PubMed: 28117917]

Escorihuela RM, Vallina IF, Martinez-Cue C, Baamonde C, Dierssen M, Tobena A, Florez J, Fernandez-Teruel A, 1998 Impaired short- and long-term memory in Ts65Dn mice, a model for down syndrome. Neurosci. Lett. 247, 171–174. [PubMed: 9655620]

Feinstein DL, Heneka MT, Gavrilyuk V, Dello Russo C, Weinberg G, Galea E, 2002 Noradrenergic regulation of inflammatory gene expression in brain. Neurochem. Int. 41, 357–365. [PubMed: 12176079]

Feinstein DL, Kalinin S, Braun D, 2016 Causes, consequences, and cures for neuroinflammation mediated via the locus coeruleus: noradrenergic signaling system. J. Neurochem. 139 (Suppl. 2), 154–178. [PubMed: 26968403]

Fortress AM, Hamlett ED, Vazey EM, Aston-Jones G, Cass WA, Boger HA, Granholm AC, 2015 Designer receptors enhance memory in a mouse model of down syndrome. J. Neurosci. 35, 1343–1353. [PubMed: 25632113]

Fructuoso M, Rachdi L, Philippe E, Denis RG, Magnan C, Le Stunff H, Janel N, Dierssen M, 2018 Increased levels of inflammatory plasma markers and obesity risk in a mouse model of down syndrome. Free Radic. Biol. Med. 114, 122–130. [PubMed: 28958596]

German DC, Manaye KF, White CL 3rd, Woodward DJ, McIntire DD, Smith WK, Kalaria RN, Mann DM, 1992 Disease-specific patterns of locus coeruleus cell loss. Ann. Neurol. 32, 667–676. [PubMed: 1449247]

Gilbert CE, Zuckerman DM, Currier PL, Machamer CE, 2014 Three basic residues of intracellular loop 3 of the beta-1 adrenergic receptor are required for golgin-160-dependent trafficking. Int. J. Mol. Sci 15, 2929–2945. [PubMed: 24566136]

Godridge H, Reynolds GP, Czudek C, Calcutt NA, Benton M, 1987 Alzheimer-like neurotransmitter deficits in adult Down's syndrome brain tissue. J. Neurol. Neurosurg. Psychiatry 50, 775–778. [PubMed: 2440994]

Granholm AS, Sanders LA, Crnic LS, 2000 Loss of cholinergic phenotype in basal forebrain coincides with cognitive decline in a mouse model of Down's syndrome. Exp. Neurol. 161, 647–663. [PubMed: 10686084]

Guettier JM, Gautam D, Scarselli M, Ruiz de Azua I, Li JH, Rosemond E, Ma X, Gonzalez FJ, Armbruster BN, Lu H, Roth BL, Wess J, 2009 A chemical-genetic approach to study G protein regulation of beta cell function in vivo. Proc. Natl. Acad. Sci. U. S. A. 106, 19197–19202. [PubMed: 19858481]

Gyoneva S, Traynelis SF, 2013 Norepinephrine modulates the motility of resting and activated microglia via different adrenergic receptors. J. Biol. Chem. 288, 15291–15302. [PubMed: 23548902]

Haglund M, Sjobeck M, Englund E, 2006 Locus ceruleus degeneration is ubiquitous in Alzheimer's disease: possible implications for diagnosis and treatment. Neuropathology 26, 528–532. [PubMed: 17203588]

Hamdani N, van der Velden J, 2009 Lack of specificity of antibodies directed against human beta-adrenergic receptors. Naunyn Schmiedeberg's Arch. Pharmacol. 379, 403–407. [PubMed: 19156400]

Hamlett ED, Boger HA, Ledreux A, Kelley CM, Mufson EJ, Falangola MF, Guilfoyle DN, Nixon RA, Patterson D, Duval N, Granholm AC, 2016 Cognitive impairment, neuroimaging, and Alzheimer neuropathology in mouse models of down syndrome. Curr. Alzheimer Res. 13, 35–52. [PubMed: 26391050]

Holtzman DM, Santucci D, Kilbridge J, Chua-Couzens J, Fontana DJ, Daniels SE, Johnson RM, Chen K, Sun Y, Carlson E, Alleva E, Epstein CJ, Mobley WC, 1996 Developmental abnormalities and age-related neurodegeneration in a mouse model of down syndrome. Proc. Natl. Acad. Sci. U. S. A. 93, 13333–13338. [PubMed: 8917591]

Hunter CL, Isacson O, Nelson M, Bimonte-Nelson H, Seo H, Lin L, Ford K, Kindy MS, Granholm AC, 2003 Regional alterations in amyloid precursor protein and nerve growth factor across age in a mouse model of Down's syndrome. Neurosci. Res. 45, 437–445. [PubMed: 12657457]

Hunter C, Bachman D, Granholm AC, 2004 11 Minocycline prevents cholinergic loss in a mouse model of Down's syndrome. Ann. Neurol. 56 (5), 675–688. [PubMed: 15468085]

Hwang DY, Carlezon WA Jr., Isacson O, Kim KS, 2001 A high-efficiency synthetic promoter that drives transgene expression selectively in noradrenergic neurons. Hum. Gene Ther. 12, 1731–1740. [PubMed: 11560767]

Illouz T, Madar R, Biragyn A, Okun E, 2019 Restoring microglial and astroglial homeostasis using DNA immunization in a down syndrome mouse model. Brain Behav. Immun. 75, 163–180. [PubMed: 30389461]

Jensen BC, Swigart PM, Simpson PC, 2009 Ten commercial antibodies for alpha-1-adrenergic receptor subtypes are nonspecific. Naunyn Schmiedeberg's Arch. Pharmacol. 379, 409–412. [PubMed: 18989658]

Kalaria RN, Andorn AC, Tabaton M, Whitehouse PJ, Harik SI, Unnerstall JR, 1989 Adrenergic receptors in aging and Alzheimer's disease: increased beta 2-receptors in prefrontal cortex and hippocampus. J. Neurochem. 53, 1772–1781. [PubMed: 2553864]

Kalinin S, Gavrilyuk V, Polak PE, Vasser R, Zhao J, Heneka MT, Feinstein DL, 2007 Noradrenaline deficiency in brain increases beta-amyloid plaque burden in an animal model of Alzheimer's disease. Neurobiol. Aging 28, 1206–1214. [PubMed: 16837104]

Kane GA, Vazey EM, Wilson RC, Shenhav A, Daw ND, Aston-Jones G, Cohen JD, 2017 Increased locus coeruleus tonic activity causes disengagement from a patch-foraging task. Cogn. Affect Behav. Neurosci. 17, 1073–1083. [PubMed: 28900892]

Kelly SC, He B, Perez SE, Ginsberg SD, Mufson EJ, Counts SE, 2017 Locus coeruleus cellular and molecular pathology during the progression of Alzheimer's disease. Acta. Neuropathol. Commun. 5, 8. [PubMed: 28109312]

Khakpour-Taleghani B, Lashgari R, Motamedi F, Naghdi N, 2009 Effect of reversible inactivation of locus ceruleus on spatial reference and working memory. Neuroscience 158, 1284–1291. [PubMed: 19041693]

Kinnavane L, Amin E, Olarte-Sánchez CM, Aggleton JP, 2016 11 Detecting and discriminating novel objects: the impact of perirhinal cortex disconnection on hippocampal activity patterns. Hippocampus 26 (11), 1393–1413. [PubMed: 27398938]

Kong Y, Ruan L, Qian L, Liu X, Le Y, 2010 Norepinephrine promotes microglia to uptake and degrade amyloid beta peptide through upregulation of mouse formyl peptide receptor 2 and induction of insulin-degrading enzyme. J. Neurosci. 30, 11848–11857. [PubMed: 20810904]

Lai F, 1992 Clinicopathologic features of Alzheimer disease in down syndrome. Prog. Clin. Biol. Res. 379, 15–34. [PubMed: 1409742]

Lai F, Williams RS, 1989 A prospective study of Alzheimer disease in down syndrome. Arch. Neurol. 46, 849–853. [PubMed: 2527024]

Langlais PJ, Connor DJ, Thal L, 1993 Comparison of the effects of single and combined neurotoxic lesions of the nucleus basalis magnocellularis and dorsal noradrenergic bundle on learning and memory in the rat. Behav. Brain Res 54, 81–90. [PubMed: 8504014]

Lein ES, et al., 2007 Allen mouse brain atlas. Genome-wide atlas of gene expression in the adult mouse brain. Nature 445, 168–176. [PubMed: 17151600]

Lockrow JB, Boger H, Bimonte-Nelson H, Granholm AC, 2011a Effects of long-term memantine on memory and neuropathology in Ts65Dn mice, a model for Down syndrome. Behav. Brain Res. 221, 610–622. [PubMed: 20363261]

Lockrow J, Boger H, Gerhardt G, Aston-Jones G, Bachman D, Granholm AC, 2011b A noradrenergic lesion exacerbates neurodegeneration in a down syndrome mouse model. J. Alzheimers Dis. 23, 471–489. [PubMed: 21098982]

Lockrow J, Fortress A, Granholm AC, 2012 Age-related neurodegeneration and memory loss in down syndrome. Curr. Gerontol. Geriatr. Res. 2012, 463909. [PubMed: 22545043]

Lopez AJ, Kramar E, Matheos DP, White AO, Kwapis J, Vogel-Ciernia A, Sakata K, Espinoza M, Wood MA, 2016 Promoter-specific effects of DREADD modulation on hippocampal synaptic plasticity and memory formation. J. Neurosci. 36, 3588–3599. [PubMed: 27013687]

Mahler SV, Aston-Jones G, 2018 CNO evil? Considerations for the use of DREADDs in Behavioral neuroscience. Neuropsychopharmacology 43, 934–936. [PubMed: 29303143]

Mahler SV, Vazey EM, Beckley JT, Keistler CR, McGlinchey EM, Kaufling J, Wilson SP, Deisseroth K, Woodward JJ, Aston-Jones G, 2014 Designer receptors show role for ventral pallidum input to ventral tegmental area in cocaine seeking. Nat. Neurosci. 17, 577–585. [PubMed: 24584054]

Mann DM, Yates PO, Marcyniuk B, 1984a A comparison of changes in the nucleus basalis and locus caeruleus in Alzheimer's disease. J. Neurol. Neurosurg. Psychiatry 47, 201–203. [PubMed: 6707659]

Mann DM, Yates PO, Marcyniuk B, 1984b Alzheimer's presenile dementia, senile dementia of Alzheimer type and Down's syndrome in middle age form an age related continuum of pathological changes. Neuropathol. Appl. Neurobiol. 10, 185–207. [PubMed: 6234474]

Manvich DF, Webster KA, Foster SL, Farrell MS, Ritchie JC, Porter JH, Weinshenker D, 2018 The DREADD agonist clozapine N-oxide (CNO) is reverse-metabolized to clozapine and produces clozapine-like interoceptive stimulus effects in rats and mice. Sci. Rep. 8, 3840. [PubMed: 29497149]

Mather M, Harley CW, 2016 The locus Coeruleus: essential for maintaining cognitive function and the aging brain. Trends Cogn. Sci. 20, 214–226. [PubMed: 26895736]

McCall JG, Al-Hasani R, Siuda ER, Hong DY, Norris AJ, Ford CP, Bruchas MR, 2015 CRH engagement of the locus Coeruleus noradrenergic system mediates stress-induced anxiety. Neuron 87, 605–620. [PubMed: 26212712]

Menendez M, 2005 Down syndrome, Alzheimer's disease and seizures. Brain and Development 27, 246–252. [PubMed: 15862185]

Nguyen R, Morrissey MD, Mahadevan V, Cajanding JD, Woodin MA, Yeomans JS, Takehara-Nishiuchi K, Kim JC, 2014 Parvalbumin and GAD65 interneuron inhibition in the ventral hippocampus induces distinct behavioral deficits relevant to schizophrenia. J. Neurosci. 34, 14948–14960. [PubMed: 25378161]

Paxinos G, Franklin K, 2001 The Mouse Brain in Stereotaxic Coordinates, 2nd edition Academic Press.

Perez DM, DeYoung MB, Graham RM, 1993 Coupling of expressed alpha 1B- and alpha 1D-adrenergic receptor to multiple signaling pathways is both G protein and cell type specific. Mol. Pharmacol. 44, 784–795. [PubMed: 8232229]

Pullar CE, Grahn JC, Liu W, Isseroff RR, 2006 Beta2-adrenergic receptor activation delays wound healing. FASEB J. 20, 76–86. [PubMed: 16394270]

Rangaraju S, Dammer EB, Raza SA, Rathakrishnan P, Xiao H, Gao T, Duong DM, Pennington MW, Lah JJ, Seyfried NT, Levey AI, 2018 Identification and therapeutic modulation of a pro-inflammatory subset of disease-associated-microglia in Alzheimer's disease. Mol. Neurodegener. 13, 24. [PubMed: 29784049]

Reeves RH, Irving NG, Moran TH, Wohn A, Kitt C, Sisodia SS, Schmidt C, Bronson RT, Davisson MT, 1995 A mouse model for down syndrome exhibits learning and behaviour deficits. Nat. Genet. 11, 177–184. [PubMed: 7550346]

Reynolds GP, Godridge H, 1985 Alzheimer-like brain monoamine deficits in adults with Down's syndrome. Lancet 2, 1368–1369.

Risser D, Lubec G, Cairns N, Herrera-Marschitz M, 1997 Excitatory amino acids and monoamines in parahippocampal gyrus and frontal cortical pole of adults with down syndrome. Life Sci. 60, 1231–1237. [PubMed: 9096240]

Roth BL, 2016 DREADDs for neuroscientists. Neuron 89, 683–694. [PubMed: 26889809]

Rueden CT, Schindelin J, Hiner MC, DeZonia BE, Walter AE, Arena ET, Eliceiri KW, 2017 ImageJ2: ImageJ for the next generation of scientific image data. BMC Bioinformatics 18, 529. [PubMed: 29187165]

Salehi A, Faizi M, Colas D, Valletta J, Laguna J, Takimoto-Kimura R, Kleschevnikov A, Wagner SL, Aisen P, Shamloo M, Mobley WC, 2009 11 18 Restoration of norepinephrine-modulated contextual memory in a mouse model of down syndrome. Sci. Transl. Med 1 (7), 7ra17 10.1126/scitranslmed.3000258.

Sansevero G, Begenisic T, Mainardi M, Sale A, 2016 Experience-dependent reduction of soluble beta-amyloid oligomers and rescue of cognitive abilities in middle-age Ts65Dn mice, a model of down syndrome. Exp. Neurol. 283, 49–56. [PubMed: 27288239]

Smith KS, Bucci DJ, Luikart BW, Mahler SV, 2016 DREADDS: use and application in behavioral neuroscience. Behav. Neurosci. 130, 137–155. [PubMed: 26913540]

Theofilas P, Ehrenberg AJ, Dunlop S, Di Lorenzo Alho AT, Nguy A, Leite REP, Rodriguez RD, Mejia MB, Suemoto CK, Ferretti-Rebustini REL, Polichiso L, Nascimento CF, Seeley WW, Nitrini R, Pasqualucci CA, Jacob Filho W, Rueb U, Neuhaus J, Heinsen H, Grinberg LT, 2017 Locus coeruleus volume and cell population changes during Alzheimer's disease progression: a stereological study in human postmortem brains with potential implication for early-stage biomarker discovery. Alzheimers Dement. 13, 236–246. [PubMed: 27513978]

Theofilas P, et al., 2018 Probing the correlation of neuronal loss, neurofibrillary tangles, and cell death markers across the Alzheimer's disease Braak stages: a quantitative study in humans. Neurobiol. Aging 61, 1–12. [PubMed: 29031088]

Trotta MB, Serro Azul JB, Wajngarten M, Fonseca SG, Goldberg AC, Kalil JE, 2011 Inflammatory and immunological parameters in adults with down syndrome. Immun. Ageing 8, 4. [PubMed: 21496308]

Uys MM, Shahid M, Harvey BH, 2017 Therapeutic potential of selectively targeting the alpha2C-adrenoceptor in cognition, depression, and schizophrenia-new developments and future perspective. Front Psychiatry 8, 144. [PubMed: 28855875]

Vazey EM, Aston-Jones G, 2014 Designer receptor manipulations reveal a role of the locus coeruleus noradrenergic system in isoflurane general anesthesia. Proc. Natl. Acad. Sci. U. S. A. 111, 3859–3864. [PubMed: 24567395]

Wang Z, Phan T, Storm DR, 2011 The type 3 adenylyl cyclase is required for novel object learning and extinction of contextual memory: role of cAMP signaling in primary cilia. J. Neurosci. 31, 5557–5561. [PubMed: 21490195]

Wisniewski K, Wisniewski H, Wen G, 1985a Occurrence of neuropathological changes and dementia of Alzheimer's disease in Down's syndrome. Ann. Neurol. 17, 278–282. [PubMed: 3158266]

Wisniewski KE, Dalton AJ, McLachlan C, Wen GY, Wisniewski HM, 1985b Alzheimer's disease in Down's syndrome: clinicopathologic studies. Neurology 35, 957–961. [PubMed: 3159974]

Xu H, Rajsombath MM, Weikop P, Selkoe DJ, 2018 Enriched environment enhances beta-adrenergic signaling to prevent microglia inflammation by amyloid-beta. EMBO Mol Med 10.

Yates CM, Ritchie IM, Simpson J, Maloney AF, Gordon A, 1981 Noradrenaline in Alzheimer-type dementia and down syndrome. Lancet 2, 39–40.

Yi B, Jahangir A, Evans AK, Briggs D, Ravina K, Ernest J, Farimani AB, Sun W, Rajadas J, Green M, Feinberg EN, Pande VS, Shamloo M, 2017 Discovery of novel brain permeable and G protein-biased beta-1 adrenergic receptor partial agonists for the treatment of neurocognitive disorders. PLoS One 12, e0180319. [PubMed: 28746336]

Zigman WB, 2013 Atypical aging in down syndrome. Dev Disabil Res Rev 18, 51–67. [PubMed: 23949829]

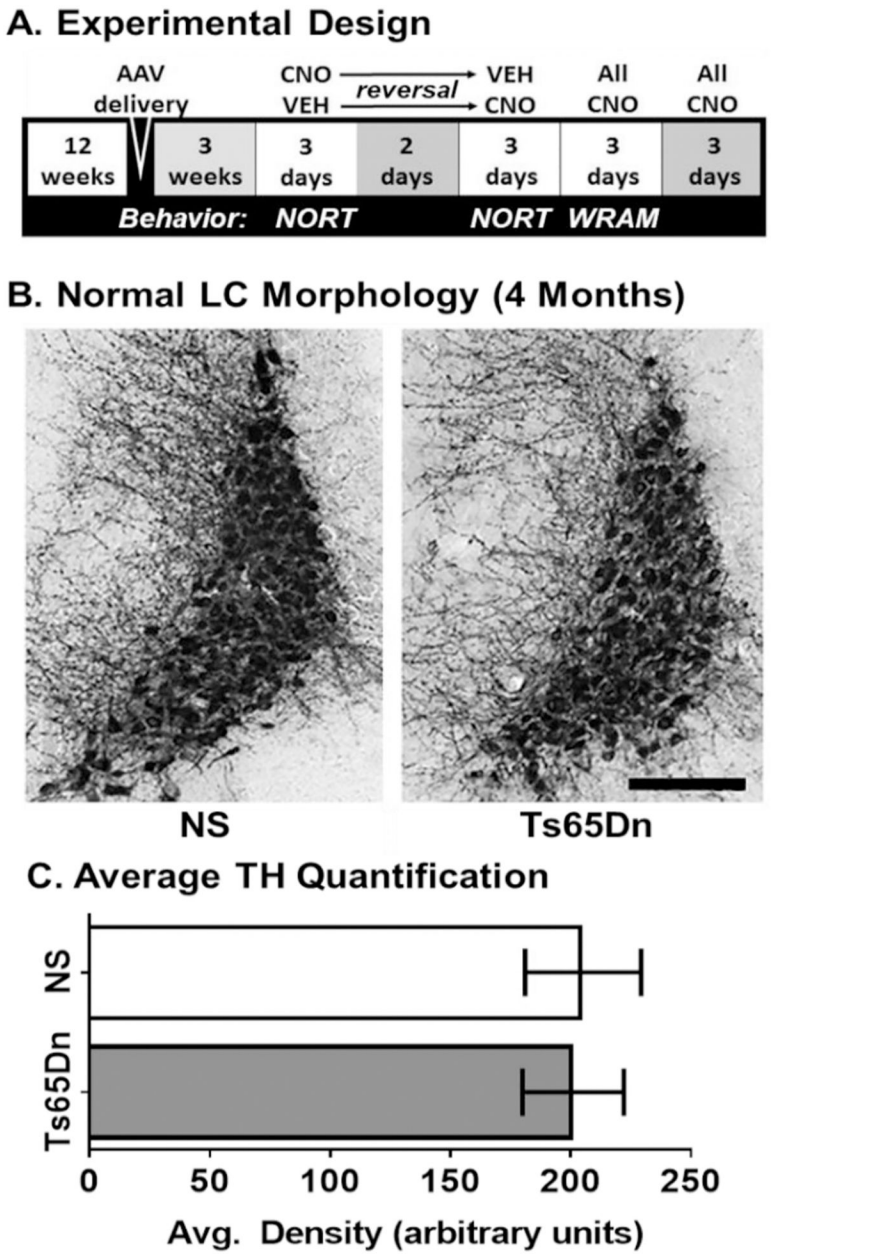

Fig. 1.

A) Experimental design. Schematic representation of the cross-treatment design employed, where CNO or saline was given to a subset of AAV-hM4Di or AAV-GFP control injected mice, followed by locomotor and NORT tasks. After a wash-out period of 2 days, the treatment paradigms were reversed, and the same behavioral assessments employed. Then all mice received CNO and were tested on the WRAM task, including a platform switch on the last day. B—C) TH DAB immunostaining in the LC-NE. At four months of age, there were no observable morphological differences in terms of TH staining morphology or density of LC cells between NS and Ts65Dn mice (Scale bar = 200 μm). Error bars represent the mean ± SEM.

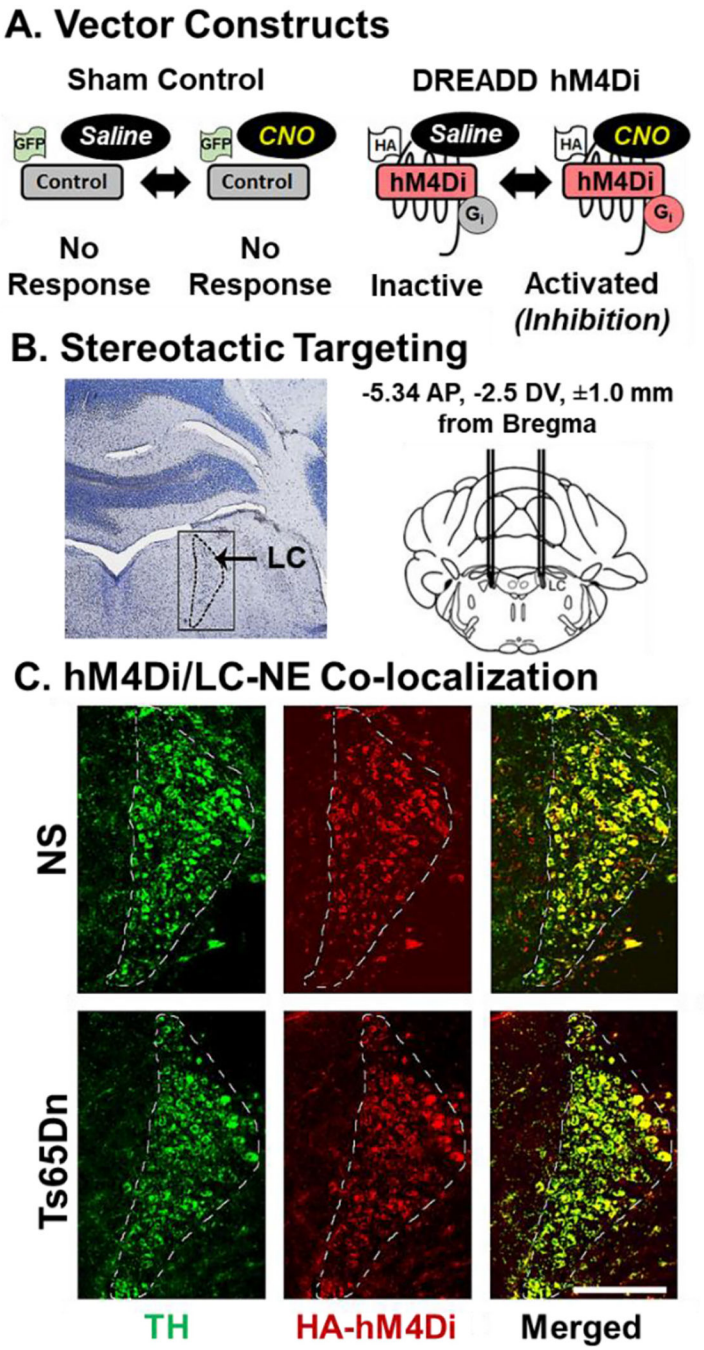

Fig. 2.

A) Vector construct. Administration of CNO will not elicit a response in the Control GFP vector while activating the hM4Di vector results in neuronal inhibition. The HA tag allows for IF visualization of the hM4Di receptor in the brain. B) Stereotactic Targeting. Bilateral stereotactic injection of viral particles in the LC using optimized coordinates. C) DREADD hM4Di/LC-NE Colocalization. TH immunostaining (green), HA staining (red), and overlay (yellow) in a representative NS and Ts65Dn mouse. (Scale bar = 250 μm). hM4Di transduction efficiency was quantified to be above 95% with 4–5 random sections in 3–4

mice per cohort. (For interpretation of the references to colour in this figure legend, the reader is referred to the web version of this article.)

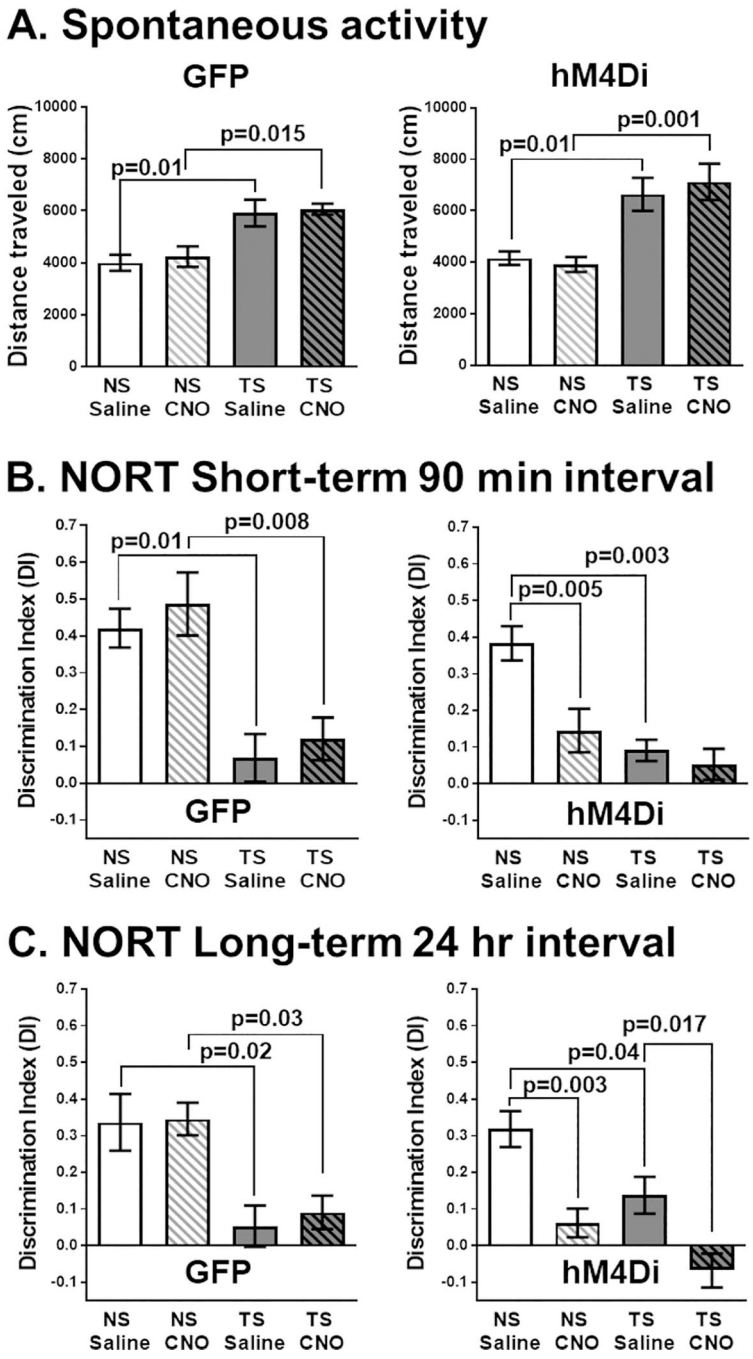

Fig. 3.

(**A**) Spontaneous motor activity. Ts65Dn mice exhibited a significant increase in total distance traveled (cm), which was not affected by CNO treatment either in AAV hM4Di or AAV GFP injected mice. The main effect was attributable to karyotype alone in GFP ($F1,16 = 24.9$, $p = .0001$) and in hM4Di groups ($F1,32 = 25.2$, $p < .0001$). (**B**) Novel Object Recognition (90 min. interval). Ts65Dn mice already had a significant deficit in this task compared to NS mice while CNO administration to the NS hM4Di group completely abrogated performance. The main effect was attributable to karyotype alone in GFP (F1,14 =

29.49, p < .0001) and to both karyotype (F1,34 = 18.25, p = .0001) and treatment (F1,34 = 9.46, p = .004) in hM4Di groups. (**C**) Novel Object Recognition (24-h interval). Ts65Dn mice already had a significant deficit in this task compared to NS mice while CNO administration to the NS hM4Di group significantly reduced performance. The main effect was attributable to karyotype alone in GFP (F1,14 = 22.45, p = .0001) and to both karyotype (F1,31 = 11.01, p = .002) and treatment (F1,33 = 24.36, p < .0001) in hM4Di groups. For both intervals, CNO administration has no effect on any Control GFP cohort. Error bars represent the mean ± SEM.

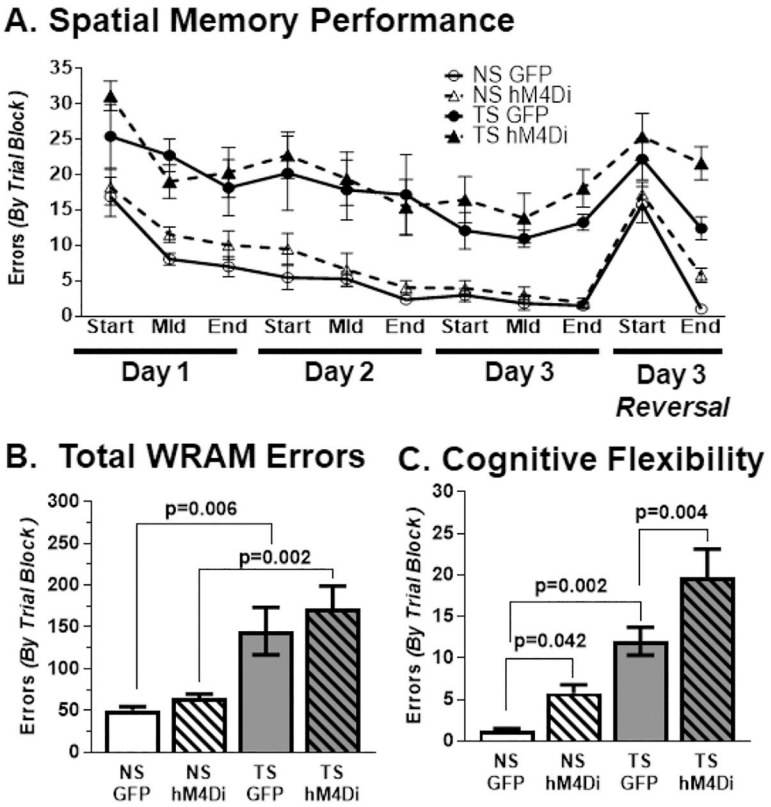

Fig. 4.

(A) WRAM Across days. DREADD hM4Di inhibition did not significantly affect spatial memory. For each day, all Ts65Dn groups made significantly more errors than their NS counterparts in every trial block. After platform switching, all mice demonstrated high error rates in finding the new hidden platform in the first trial block with variable levels of improvement in the second trial block. **(B) Total WRAM errors.** Ts65Dn mice performed significantly worse than their NS counterparts and LC inhibition did not affect overall performance relative to the GFP control cohorts. The main effect was attributable to karyotype ($F1,23 = 20.37$, $p = .0002$). **(C) Cognitive Flexibility.** NS GFP made significantly fewer errors than Ts65Dn GFP and hM4Di inhibition of the LC led to a significant increase in errors for both NS and Ts65Dn mice. The main effects were attributable to karyotype ($F1,23 = 53.82$, $p < .0001$) and treatment ($F1,23 = 22.36$, $p < .0001$). Error bars represent the mean ± SEM.

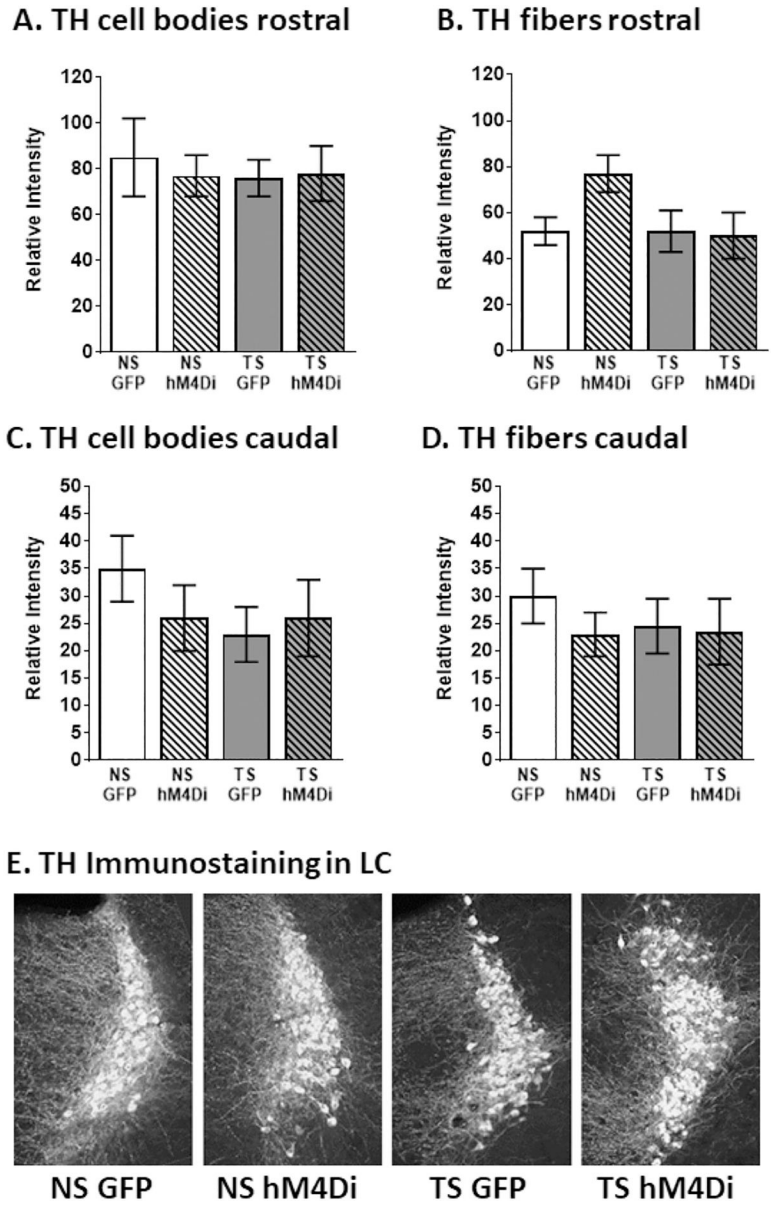

Fig. 5.

LC inhibition did not significantly affect TH staining in any cohort when examined by **cell body density** for **(A) rostral** and **(B) caudal,** or in LC fibers density for **(C) rostral** and **(D) caudal.** Examination of the **(E) Gross morphology** between each cohort demonstrates that the LC appears equivalent between all groups. Error bars represent the mean ± SEM.

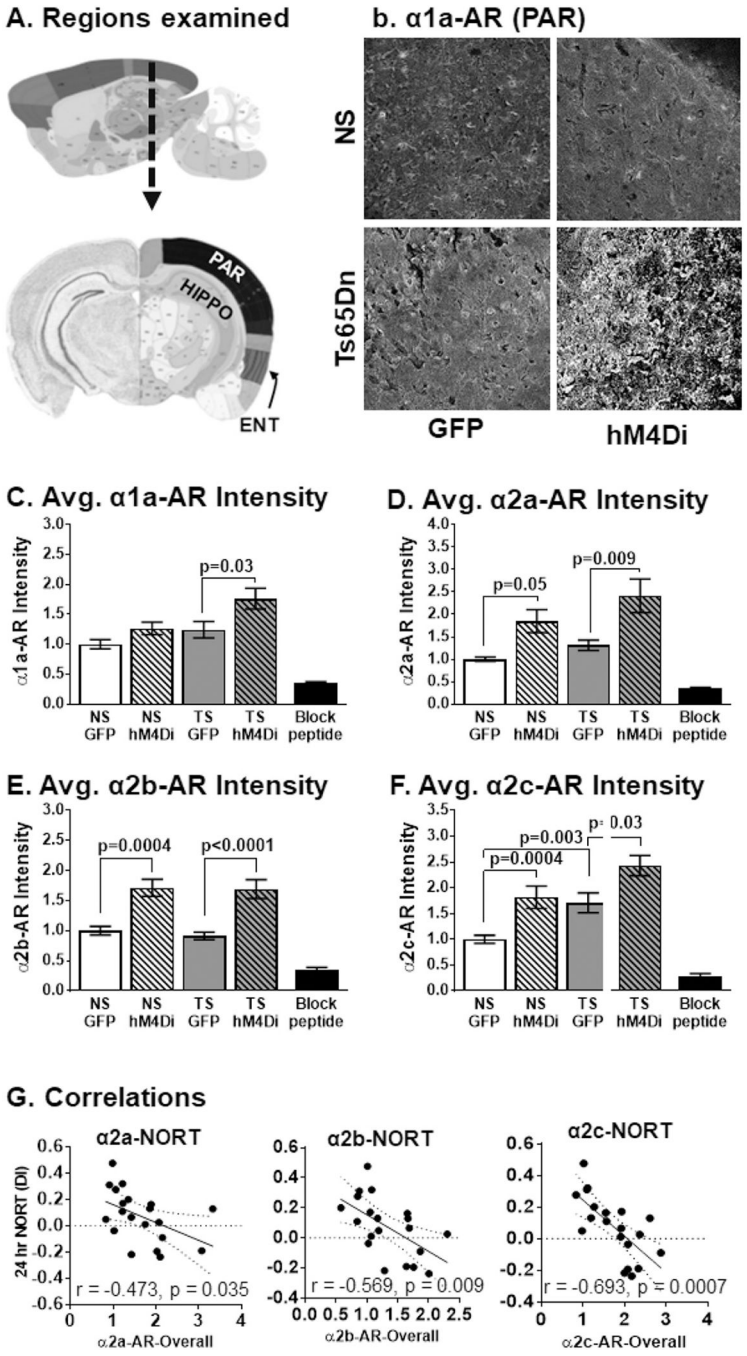

Fig. 6.

α-ARs immunostaining in response to DREADD hM4Di inhibition of the LC. For all α-ARs, the main effects were attributable to treatment since compensatory receptor expressions were seen in **(A)** Regions examined by α-AR IF. Representative immunofluorescence for α1a-AR comparing all cohorts (parietal region) **(B)**. Normalized fluorescent intensities for **(C)** α1a-AR ($F_{1,56} = 9.45$, $p = .003$), **(D)** α2a-AR ($F_{1,56} = 17.2$, $p = .0001$), **(E)** α2b-AR ($F_{1,44} = 43.91$, $p < .0001$) and **(F)** α2c-AR ($F_{1,44} = 26.40$, $p < .0001$). A significant effect could also be attributed to karyotype in α1a-AR ($F_{1,56} = 8.40$,

p = .005), and α2c-AR (F1,44 = 17.73, p = .0001). Scale bar = 100 μm. **(G)** Expression levels of α2a-, α2b- and α2c-ARs negatively correlated with 24-h NORT DI performance. Error bars represent the mean ± SEM. Dotted lines represented the 95% confidence interval.

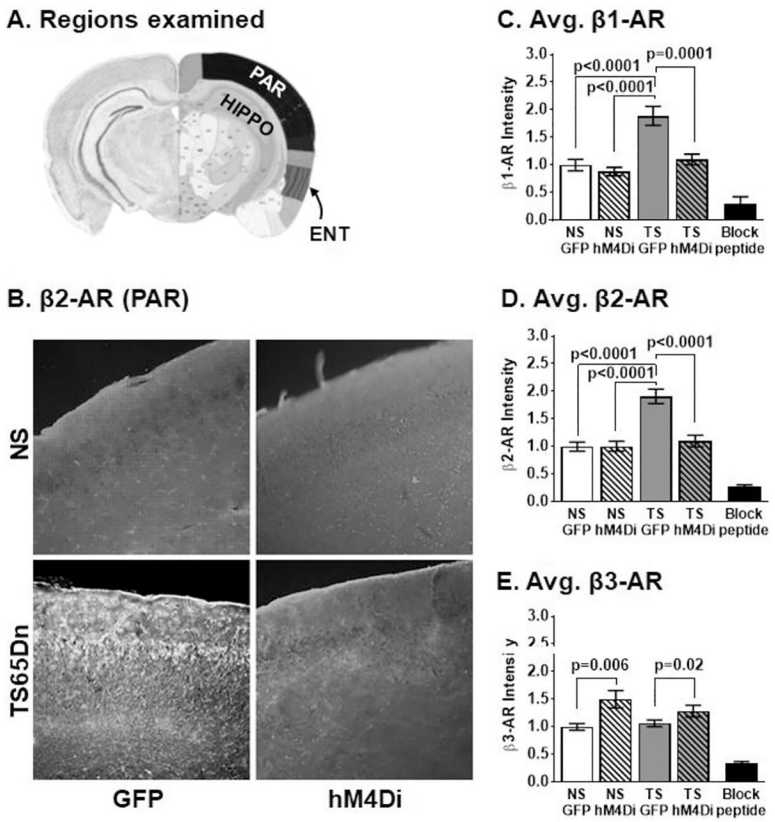

Fig. 7.

(A) Regions examined by β-AR IF. **(B)** Representative images that compare β2-AR response to DREADD hM4Di inhibition of the LC. β1-and β2-AR are already elevated in Ts65Dn mice. For β1-AR **(C),** the main effects were attributable to karyotype ($F_{1,44} = 22.36$, $p < .0001$) and treatment ($F_{1,44} = 14.86$, $p = .0004$) with significant interaction ($F_{1,44} = 8.14$, $p = .007$) since the treatment effect was only observed in Ts65Dn hM4Di inhibition of the LC normalized on Ts65Dn levels to that observed in NS mice. For β2-AR **(D),** the main effects were attributable to karyotype ($F_{1,53} = 22.31$, $p < .0001$) and treatment ($F_{1,44} = 14.21$, $p = .0004$) with significant interaction ($F_{1,44} = 14.75$, $p = .0003$). For β3-AR **(E)** the main effects were attributable to treatment ($F_{1,56} = 12.15$, $p = .001$) since hM4Di inhibition of the LC resulted in compensatory elevations. The most profound changes of LC inhibition were observed in the entorhinal cortical regions for β1-AR (D), β2-AR (E) and β3-AR (E) (Scale bar = 100 μm). Error bars represent the mean ± SEM.

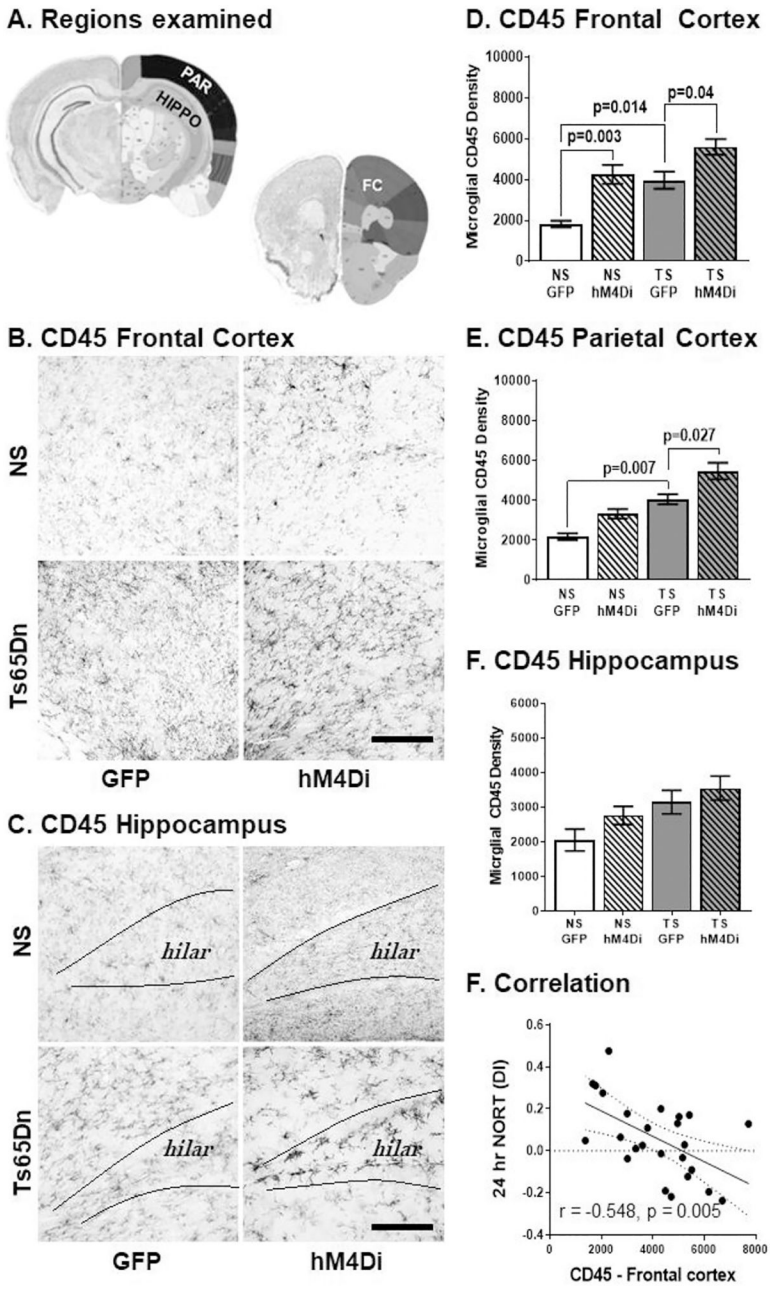

Fig. 8.

(A) Regions examined. Microglial CD45 immunostaining in response to DREADD hM4Di inhibition of the LC. CD45 DAB intensity was already elevated in Ts65Dn mice in the frontal cortex (B) and in the hippocampus (C). hM4Di inhibition of the LC significantly elevated CD45 levels in the brain for both NS and Ts65Dn mice. In the frontal cortex (D) the main effects were attributable to karyotype ($F_{1,21} = 18.06$, $p = .0004$) and treatment ($F_{1,21} = 24.45$, $p < .0001$). (Scale bar = 250 μm). In the parietal cortex (E), the main effects were attributable to karyotype ($F_{1,21} = 37.09$, $p < .0001$) and treatment ($F_{1,21} = 15.11$, $p = .0009$). In the hippocampus (E), the main effects were attributable to karyotype alone ($F_{1, 20} = 8.7$, $p = .007$). Error bars represent the mean ± SEM. (F) Correlations. CD45

expression levels in frontal cortex negatively correlated with 24 h NORT DI performance. Dotted lines represented the 95% confidence interval.